Results in Physics 12 (2019) 738–742

Contents lists available at ScienceDirect

Results in Physics

journal homepage: www.elsevier.com/locate/rinp

Effect of SO_4^{2-} and Cl^- anionic attack on the localized corrosion resistance and morphology of 409 ferritic stainless steel

Roland Tolulope Loto

Department of Mechanical Engineering, Covenant University, Ota, Ogun State, Nigeria

ARTICLE INFO

Keywords:
Pitting
Corrosion
Intergranular
Chloride
Anions

ABSTRACT

The corrosion polarization behaviour and optical characterization of 409 ferritic stainless steel (SS409) in 0.25 M H_2SO_4 (at specific NaCl concentration), 0.375 M H_2SO_4 and 0.5 M H_2SO_4 was evaluated with potentiodynamic polarization technique, open circuit potential measurement and optical microscopy characterization. Results showed the SS409 corrosion rate is proportional to the concentration of SO_4^{2-} and Cl^- anions in the electrolyte. At 0.25 M H_2SO_4, SS409 corroded at a rate of 7.29 mm/y; addition of 0.125% NaCl accelerated the corrosion rate to 16.75 mm/y coupled with a corresponding increase in corrosion current density from 6.71×10^{-4} Acm^2 to 3.08×10^{-3} Acm^2. Further increase in Cl^- anion concentration to 0.75% NaCl increased the corrosion rate to 19.49 mm/y. At 0.25 M H_2SO_4 the pitting current value is 1×10^{-4} A, this value increased to 1.03×10^{-4} A at 0.25 M H_2SO_4 (0.125% NaCl) and 8.40×10^{-4} A at 0.25 M H_2SO_4 (0.5% NaCl). Beyond 0.5% NaCl, passivation behavior was completely absent. Intergranular cracks, large macro-pits and numerous micro-pits were observed for SS409 from 0.25 M H_2SO_4 (0.75% NaCl) due to Cr depletion and dissolution of inclusions. SS409 from 0.5 M H_2SO_4 showed the presence of deepened intergranular cracks, shallow pits and a deteriorated surface due to the action of SO_4^{2-} anions. The morphology of SS409 in 0.25 M H_2SO_4 + 0.125% NaCl showed slight deterioration in addition to enlarged micro-pits.

Introduction

Ferritic steels belong to the class of chromium (approximately 11% and 30% Cr content), magnetic stainless steels with low carbon weight content. Other elements such as nickel, molybdenum, manganese, silicon and titanium are also present within the steel. They exhibit excellent mechanical properties such as good ductility, high corrosion resistance and relatively low susceptibility to stress corrosion cracking. Their strong resistance to oxidization in aqueous media and at high temperatures is due to the presence of silicon and aluminum within their microstructure while molybdenum provides impressive resistance to pitting and crevice corrosion in chloride containing environments. These steels possess a body-centered cubic grain structure. Grade 409 of the ferritic steel containing about 12% Cr content is a relatively low-cost derivative within this category of steels, with good formability and weldability characteristics [1]. They offer economical corrosion resistance properties with extensive application in the manufacture of automobile exhausts, mufflers, radiator tanks, catalytic converters, smoke extractors, containerization, tubular manifolds, fertilizer trunks and gas turbine exhaust silencers. However, 409 ferritic steel is less resistant to pitting corrosion, and intergranular corrosion compared to the austenitic stainless steel grades due to chromium depletion at the boundary within the steel's intermetallic phases. Pitting corrosion results from surface inclusions due to titanium additions, impurities and micro abrasions/mechanical wear especially in mild corrosive environments. Once pit initiates due to anodic dissolution and release of metal cations abundant within the pit, chloride anions are attracted to the pit reducing the pH within. This accelerates the corrosion reaction processes auto-catalytically [2]. Breakdown of the thin passive layer on ferritic steels is responsible for this process and the extent of corrosivity of the operating environment strongly influences the ability of the passive film to reform [3]. Chlorides and sulphates of varying concentration are generally encountered in the application of 409 ferritic steel and have been known to reduce the operating lifespan of these steels [4]. While previous research focused on the effect of sulphates or chlorides on ferritic steels [5]. Other research studied ferritic steel corrosion in simulated automotive exhaust system [6,7]. Lee et al. [8] studied the relationship between surface roughness and the corrosion resistance of 21Cr ferritic stainless steel and found a strong correlation between them. The corrosion resistance of ferritic steel studied in concentrated alkaline solution showed that decrease in pH enabled passive film formation [9]. Appropriate selection of ferritic steels with respect to corrosivity of the operating environment is one of the factors in sustaining the viability of ferritic steels in service; another important

E-mail address: tolu.loto@gmail.com.

https://doi.org/10.1016/j.rinp.2018.12.031
Received 16 October 2018; Received in revised form 5 December 2018; Accepted 7 December 2018
Available online 11 December 2018

Table 1
Percentage Nominal Composition of SS409.

Element Symbol	S	Si	Ni	Cr	Mn	P	N	Ti	C	Fe
% Composition SS409	0.045	1	1.8	11.75	1	0.045	0.5	0.75	0.08	83.03

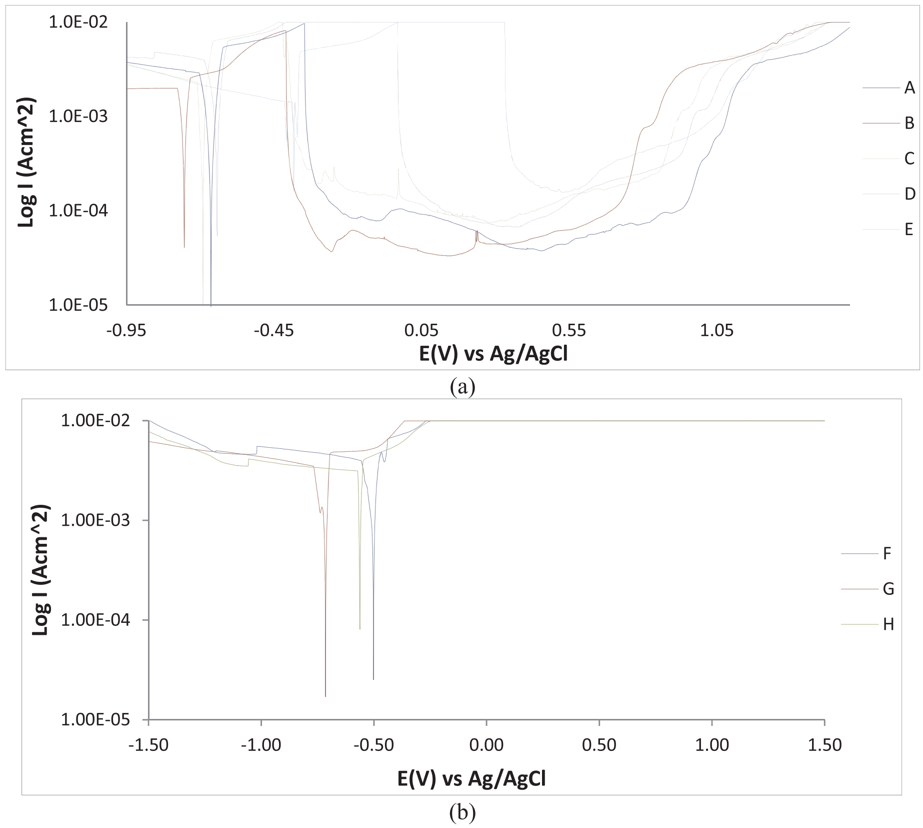

Fig. 1. Anodic-cathodic polarization plot for SS409 (a) 0.25 M H_2SO_4, 0.25 M H_2SO_4 + 0.125% NaCl, 0.25 M H_2SO_4 + 0. 25% NaCl, 0.25 M H_2SO_4 + 0.375% NaCl and 0.25 M H_2SO_4 + 0.5% NaCl solutions, and (b) 0.25 M H_2SO_4 + 0.75% NaCl, 0.375 M H_2SO_4 and 0.5 M H_2SO_4 solutions.

factor is the use of corrosion inhibitors [10,11]. This research focuses on the synergistic corrosive effect of chlorides, sulphates and their threshold equilibrium value on the passivation behavior and localized corrosion resistance of 409 ferritic stainless steel.

Experimental methods

409 ferritic stainless steel (SS409) obtained from an automobile exhaust muffler is the candidate alloy for the research. The ferritic steel was characterized at the Materials Characterization Laboratory, Department of Mechanical Engineering, Covenant, Ogun State, Nigeria. Data on the elemental composition from characterization are detailed in Table 1. The steel samples were cut, sectioned and machined to dimensions with unconcealed surface area of 2 cm^2. Abrasive silicon carbide papers with grits of 60, 120, 220, 320, 600 and 800 were used to grind the steel specimens before polishing to 6 µm with diamond paste. The samples were subsequently washed with deionized water and acetone for potentiodynamic polarization and open circuit potential measurement electrochemical tests. Analar grade sodium chloride purchased from Titan Biotech, India and sulphuric acid (98%) purchased from Sigma Aldrich, USA were formulated in molar concentrations of 0.25 M H_2SO_4, 0.25 M H_2SO_4 + 0.125% NaCl, 0.25 M H_2SO_4 + 0.25% NaCl, 0.25 M H_2SO_4 + 0.375% NaCl, 0.25 M H_2SO_4 + 0.5% NaCl, 0.25 M H_2SO_4 + 0.75% NaCl, 0.375 M H_2SO_4 and 0.5 M H_2SO_4 in 200 mL of the acid solution.

Electrochemical test by potentiodynamic polarization was performed on SS409 at 37 °C ambient temperature with the aid of platinum counter electrodes, Ag/AgCl reference electrodes and resin embedded SS409 electrodes placed within a transparent container filled with 200 mL of the acid chloride electrolyte at the concentrations earlier stated. The electrodes were interfaced with Digi-Ivy 2311 potentiostat connected to a computer. Anodic-cathodic polarization curves were produced at scan rate of 0.0015 V/s from −1.5 V and +1.5 V set potentials. Corrosion current density, C_d (A/cm^2) and corrosion potential, C_p (V) values were obtained from the intercept of the polarization curves through Tafel extrapolation method. Corrosion rate, C_R (mm/y) and inhibition efficiency, η (%) was calculated from the formula below;

$$C_R = \frac{0.00327 \times C_d \times E_q}{D} \quad (1)$$

D is the density in (g/cm^3); E_q is the steel equivalent weight (g). 0.00327 is the constant for corrosion rate. Open circuit potential measurement (OCP) was performed at 0.05 V/s step potential for 3200 s to study the thermodynamic stability of the alloys at rest potentials. Micro analytical images of the duplex alloys surface configuration were studied before and after electrochemical degradation with Omax trinocular metallurgical microscope using ToupCam analytical software.

Table 2
Potentiodynamic polarization data for SS409 in solution concentrations from 0.25 M H_2SO_4 – 0.5 M H_2SO_4.

Sample	Solution Conc. (%)	Corrosion Rate (mm/y)	Corrosion Current (A)	Corrosion Current Density (A/cm^2)	Corrosion Potential (V)	Polarization Resistance, R_p (Ω)	Cathodic Tafel Slope, B_c (V/dec)	Anodic Tafel Slope B_a (V/dec)
A	0.25 M H_2SO_4	7.29	1.34E−03	6.71E−04	−0.664	19.15	−0.480	0.542
B	0.25 M H_2SO_4 + 0.125% NaCl	16.75	3.08E−03	1.54E−03	−0.754	8.34	−0.460	0.489
C	0.25 M H_2SO_4 + 0.25% NaCl	17.09	3.14E−03	1.57E−03	−0.691	9.07	−0.761	0.556
D	0.25 M H_2SO_4 + 0.375% NaCl	17.57	3.23E−03	1.62E−03	−0.643	7.95	−0.706	0.633
E	0.25 M H_2SO_4 + 0.5% NaCl	18.82	3.46E−03	1.73E−03	−0.384	7.42	−0.651	0.862
F	0.25 M H_2SO_4 + 0.75% NaCl	19.49	3.58E−03	1.79E−03	−0.502	7.17	−0.572	1.525
G	0.375 M H_2SO_4	18.96	3.49E−03	1.74E−03	−0.715	7.37	−0.442	0.673
H	0.5 M H_2SO_4	37.06	6.82E−03	3.41E−03	−0.562	3.77	−0.147	0.983

Results and discussion

Potentiodynamic polarization studies

The corrosion polarization plots of SS409 in SO_4^{2-} anion and SO_4^{2-}/Cl^- anion containing solutions are shown in Fig. 1(a) and (b). Polarization data obtained are presented in Table 2. The corrosion rates of the steel in the electrolytes studied are proportional to the concentration of SO_4^{2-} and Cl^- anions. At 0.25 M concentration of H_2SO_4, SS409 corroded at a rate of 7.29 mm/y; addition of 0.125% NaCl to the acid solution accelerated the corrosion rate to 16.75 mm/y coupled with a corresponding increase in corrosion current density from 6.71×10^{-4} Acm^2 to 3.08×10^{-3} Acm^2 (Table 2). The slight decrease in the Tafel slopes values observed at this concentration indicates an increase in the anodic dissolution and hydrogen evolution reactions associated with general and localized corrosion deterioration of the steel. Previous research has shown that Cl^- anions initiate localized corrosion most especially pitting through an autocatalytic process due to its highly reactive characteristics [12]. This involves its adsorption and electrochemical action on the steel especially at sites with weak protective oxide formation, leading to breakdown of the passive film. Cl^- anion adsorption onto SS409 surface, a charge transfer process is represented by equation below:

$$Cl^-_{(aq)} + M^+ \rightarrow Cl^-M + e^-$$

The passive film on SS409 is the product of oxidation reaction involving adsorption of oxygen atoms to form chromium rich chromium oxide [13–15]. Further increase in Cl^- anion concentration to 0.75% caused a proportionate increase in corrosion rate values to 19.49 mm/y suggesting higher Cl^- anion concentration leads to more Cl^- anion adsorption to the SS409 surface. Increase in corrosion rate is often associated with greater destruction of the passive film hence hydroxyl ion and oxygen adsorption onto the steel would have been hindered [16]. The shift in corrosion potential from −0.664 V at 0.25 M H_2SO_4 to −0.754 V at 0.25 M H_2SO_4 + 0.125% NaCl confirms the thinning/weakening of the passive film due to Cl^- anion adsorption and interaction with the underlining iron substrate. However, it was also observed that between 0.125% NaCl till 0.5% NaCl, increase in Cl^- anion concentration shifts the corrosion potential to noble values despite increase in corrosion rate. This phenomenon can be explained on the basis that reaction between the Cl^- anions and the steel results in the formation of complexes on the steel surface that further accelerates general surface deterioration of the alloy. The corrosion rate slightly decreased at 0.375 M H_2SO_4 to 18.96 mm/y. This value is higher than the corrosion rate of SS409 in SO_4^{2-}/Cl^- anion solution at 0.5% NaCl, but lower at 0.75% NaCl signifying the Cl^-/SO_4^{2-} interaction and threshold value i.e. where their action on the surface deterioration of the steel coincides. At 0.5 M H_2SO_4 solution there is a sharp increase in corrosion rate to 37.06 mm/y due to the debilitating action of SO_4^{2-} anions only. Increase in the anodic Tafel slope confirms this assertion as the adsorbed sulfate anion accelerates the mechanism of the corrosion reaction processes.

Pitting corrosion evaluation

Table 3 shows the potentiostatic variables for the localized corrosion reactions on SS409. Though these are not absolute values, they undoubtedly provide insight to the pitting mechanism during potential scanning. Cl^- and SO_4^{2-} anions within the electrolyte solutions are responsible for the localized breakdown of the passive film on the surface of SS409, though from the polarization plot in Fig. 1(a) and Table 3, it is clearly evident that increase in Cl^- anion concentration increases the tendency for pitting initiation on the steel [17,18]. Due to the active behaviour of the steel variation in corrosion potential occurs which strongly influences the pitting potential values, as a result

Table 3
Potentiostatic data for SS409 in solution concentrations from 0.25 M H_2SO_4 − 0.25 M H_2SO_4 + 0.5% NaCl.

NaCl Conc. (%)	Pitting Potential (V), E_{pitt}	Pitting Current (A)	Passivation Potential (V)	Passivation Current (A)	Passivation Range (V)	Metastable Pitting Potential (V)	Metastable Pitting Current (A)
0.25 M H_2SO_4	0.870	1.00E−04	−0.320	2.50E−04	1.190	−0.410	0.00772
0.25 M H_2SO_4 + 0.125% NaCl	0.698	1.03E−04	−0.370	1.36E−04	1.068	−0.471	0.00704
0.25 M H_2SO_4 + 0.25% NaCl	0.795	2.13E−04	−0.339	2.80E−04	1.134	−0.490	0.00823
0.25 M H_2SO_4 + 0.375% NaCl	0.857	2.91E−04	0.005	2.45E−04	0.852	−0.094	0.00994
0.25 M H_2SO_4 + 0.5% NaCl	1.017	8.40E−04	0.355	3.70E−04	0.662	0.272	0.00994

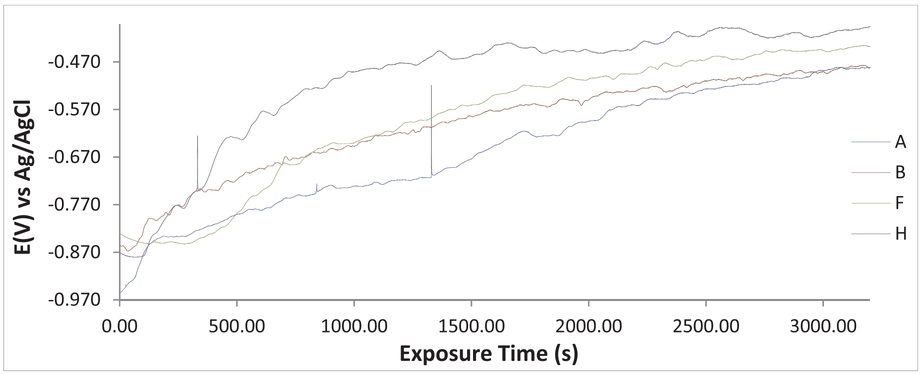

Fig. 2. Variation of OCP versus exposure time for SS409 in 0.25 M H_2SO_4, 0.25 M H_2SO_4 + 0.125% NaCl, 0.25 M H_2SO_4 + 0.75% NaCl and 0.5 M H_2SO_4.

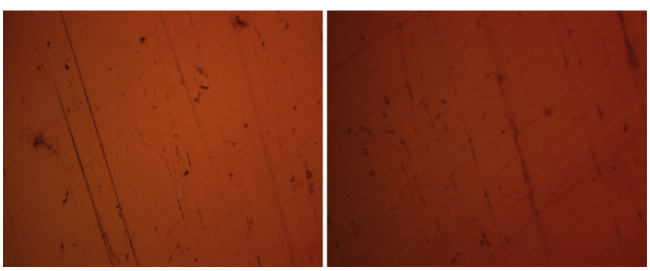

Fig. 3. Optical image of SS409 before corrosion test.

changes in pitting potential were not proportional to Cl^- anion concentration. However observation of the pitting current shows a proportionate increase in value with respect to Cl^- anion concentration. At 0.25 M H_2SO_4 (0% NaCl), the pitting current value is 1×10^{-4} A, the value increased to 1.03×10^{-4} A at 0.25 M H_2SO_4 + 0.125% NaCl and 8.40×10^{-4} A at 0.25 M H_2SO_4 + 0.5% NaCl. Beyond 0.5% NaCl, passivation behavior completely disappeared due to total destruction of the passive film by the corrosive anions, which hindered its ability to reform. The increase in corrosion current density is due to increase in Cl^- anion concentration. This invariably narrows the passive region significantly from 1.190 V (0.25 M H_2SO_4) to 0.662 V (0.25 M H_2SO_4 + 0.5% NaCl), proving Cl^- anions strongly influence the localized corrosion resistance of SS409. The decrease in passivation range results from the delayed passivation of the steel due to partial anodic dissolution reactions and subsequent metastable pitting activity as shown in the polarization plots [Fig. 1(a)] [19]. As the Cl^- anion concentration increases, the degree of anodic dissolution increases. This causes the anodic portion of the polarization plot to extend further before metastable pitting; hence the passivation range decreases signifying higher susceptibility of the steel to localized corrosion. As earlier mentioned, increase in current density due to Cl^- anion increase causes the rate of corrosion to increase rapidly which precedes pit initiation and propagation through autocatalytic mechanism resulting in hydrolysis of the substrate metal.

Open circuit potential measurement (OCP)

OCP plots for SS409 specimens (A, B, F and H) from 0.25 M H_2SO_4, 0.25 M H_2SO_4 + 0.125% NaCl, 0.25 M H_2SO_4 + 0.75% NaCl and 0.5 M H_2SO_4 solutions depicting the thermodynamic tendency of SS409 to participate in the resulting electrochemical corrosion reactions are shown in Fig. 2. Observation of the plots shows an unusual phenomenon, which contrast the results from potentiodynamic polarization. Specimen A has the lowest corrosion rate from the polarization test, yet potential values on its OCP plot were the most electronegative in the absence of applied potential. The OCP values started at −0.955 $V_{Ag/AgCl}$ (0 s) and increased progressively to −0.482 $V_{Ag/AgCl}$ at 3200 s. The same observation was recorded for specimen B and F which started at −0.859 $V_{Ag/AgCl}$ and −0.830 $V_{Ag/AgCl}$ (0 s) respectively before progressing significantly to less negative OCP values. Specimen H which had the highest corrosion rate from polarization test was relatively more electropositive throughout the exposure hours. Delineating the OCP observations, formation of passive oxide on SS409 is responsible for the differences in OCP plot. The extent of oxide formation on specimen H is much more than the other SS409 specimens due to the higher oxidizing strength of 0.5 M H_2SO_4 followed by specimen F (0.25 M H_2SO_4 + 0.75% NaCl). This shows that the surface properties of SS409 react aggressively to the presence of corrosive anions without

Fig. 4. Optical image of SS409 after corrosion test (a) 0.25 M H_2SO_4, (b) 0.25 M H_2SO_4 + 0.125% NaCl.

(a) (b)

Fig. 5. Optical image of SS409 after corrosion test (a) 0.25 M H_2SO_4 + 0.75% NaCl, (b) 0.5 M H_2SO_4.

applied potential. The lower the corrosive strength of the electrolyte, the higher the tendency of SS409 to corrode due to the thickness of the passive film formed. Secondly the higher oxide formation for sample H despite the strength of the corrosive solution could be due to the formation of oxide sulphate/oxide chloride complexes which basically confer superficial corrosion protection [20]. There is also the possibility that the oxide formation is the response of SS409 to general surface deterioration which was successfully hindered with respect to solution content and concentration but yet the steel remained prone to localized to corrosion reactions.

Microscopic image analysis

Optical images of SS409 before corrosion and after corrosion from 0.25 M H_2SO_4, 0.25 M H_2SO_4 + 0.125% NaCl, 0.25 M H_2SO_4 + 0.75% NaCl and 0.5 M H_2SO_4 solution (specimen A, B, F and G) are shown from Figs. 3–5(b). Intergranular cracks appeared at the grain boundaries of Fig. 5(a) and (b) due to Cr depletion at adjacent sites of the intermetallic phases on S409 morphology. Below the minimum Cr content necessary the passive film cannot reform. The Titanium content in SS409 according to Wang et al. [21], and Leban and Tisu [22] decreases the susceptibility of the steel to intergranular corrosion due to its stronger attraction to carbon than chromium, which in effect induce the formation of precipitates. But there is also the possibility of galvanic corrosion occurring on SS409 due to its multiphase microstructure. The multiphase microstructure of ferritic steels is also responsible for the rapid dissolution of impurities present within SS409 metallurgical structure along grain boundaries which segregates. Enlarged macro pits surrounded by numerous micro corrosion pits are quite visible on Fig. 5(a) due to the electrochemical action of excess Cl^- anions compared to Fig. 4(b) where the corrosion pits are relatively smaller though general surface deterioration of SS409 specimen also occurred. Cl^- anions enhance the corrosion mechanism responsible for pit initiation and propagation. Their small size enables diffusion through cracks on the passive film onto the substrate metal. SS409 specimen from 0.5 M H_2SO_4 [Fig. 5(b)] has had the highest corrosion rate from potentiodynamic polarization test, however its morphology showed relatively smaller but more corrosion pits compared to Fig. 5(a) due to the action of SO_4^{2-} anions in the acid media, though intergranular cracks and general surface deterioration are clearly more visible. Fig. 4(a) shows the morphology of SS409 after corrosion in 0.25 M H_2SO_4, the surface deterioration is minimal compared to Fig. 5(a). Addition of 0.125% NaCl increased the occurrence of corrosion pits and partial surface discoloration due to formation of rust resulting from corrosion.

Conclusion

409 ferritic steel withstood the effect of SO_4^{2-} anions in 0.25 M H_2SO_4 having the lowest corrosion rate value, and micro-pits appearing on its morphology at specific sites. Addition of 0.125% NaCl to the acid solution significantly deteriorated the morphology of the steel coupled with increased size and occurrence of corrosion pits. Intergranular cracks appeared at with addition of 0.75% NaCl with enlarged macro corrosion pits and significantly higher corrosion rate. At 0.5 M H_2SO_4, the corrosion rate is the highest while corrosion pits on 409 steel morphology drastically reduced to micro level. General surface deterioration and deepened intergranular cracks are visible. In the electrolytes studied the open circuit corrosion potential of 409 steel shifted positive potentials relative to solution concentration due to passive film formation. Passivation characteristics of the steel was suppressed after 0.25 M H_2SO_4 + 0.5% NaCl solution

Acknowledgement

The author of the publication is grateful to Covenant University, Ota, Ogun State, Nigeria for their support provision of research facilities.

Appendix A. Supplementary data

Supplementary data to this article can be found online at https://doi.org/10.1016/j.rinp.2018.12.031.

References

[1] Juliana S, Leandro A, Isaac JS, Renato AA. Electrochemical study of the AISI 409 ferritic stainless steel: passive film stability and pitting nucleation and growth. Mater Res 2017;20(6):1669–80. https://doi.org/10.1590/1980-5373-MR-2017-0204.
[2] Fong-Yuan M. Corrosive effects of chlorides on metals Pitting corrosion. Intech Open 2012:139–78.
[3] Oliver DC, Sephton M. External corrosion resistance of steel and ferritic stainless-steel exhaust systems. J South Afr Inst Mineral Metall 2003;103(2):93–100.
[4] Loto RT. Corrosion behavior of S43035 ferritic stainless steel in hot sulphate/chloride solution. J Mater Res Technol 2017. https://doi.org/10.1016/j.jmrt.2017.07.004.
[5] Luo H, Su H, Dong C, Xiao K, Li X. Electrochemical and passivation behavior investigation of ferritic stainless steel in simulated concrete pore media. Data Brief 2015;5:171–8.
[6] Wei LL, Chen LQ, Ma MY, Liu HL, Misra RDK. Oxidation behavior of ferritic stainless steels in simulated automotive exhaust gas containing 5 vol.% water vapor. Mater Chem Phys 2018;205:508–17.
[7] Salgado MF, Samara CSR, Santos DM, Brandim AS, Lins VFC. Cyclic oxidation resistance of ferritic stainless steels used in mufflers of automobiles. Eng Fail Anal 2017;79:89–97.
[8] Lee SM, Lee WG, Kim YH, Jang H. Surface roughness and the corrosion resistance of 21Cr ferritic stainless steel. Corros Sci 2012;63:404–9.
[9] Fattah-alhosseini A, Vafaeian S. Passivation behavior of a ferritic stainless steel in concentrated alkaline solutions. J Mater Res Technol 2015;4(4):423–8.
[10] Loto RT. Study of the synergistic effect of 2-methoxy-4-formylphenol and sodium molybdenum oxide on the corrosion inhibition of 3CR12 ferritic steel in dilute sulphuric acid. Results Phys 2017;7:769–76.
[11] Loto RT. Corrosion polarization behaviour and inhibition of S40977 stainless steel in benzosulfonazole/3 M H_2SO_4 solution. S Afr J Chem 2017;24:148–55.
[12] Loto RT. Pitting corrosion evaluation of austenitic stainless-steel type 304 in acid chloride media. J Mater Environ Sci 2013;4(4):448–59.
[13] Olatunji-Ojo O, Taylor CD. Changes in valence, coordination and reactivity that occur upon oxidation of fresh metal surfaces. Philos Mag Lett 2013;93:4283–310.
[14] Francis MF, Taylor CD. First-principles insights into the structure of the incipient magnesium oxide and its instability to decomposition: oxygen chemisorption to Mg(0001) and thermodynamic stability. Phys Rev B 2013;87:7. https://doi.org/10.1103/PhysRevB.87.075450.
[15] Francis MF, Holby E. Thermodynamics of passive film formation from first-principles. In: Taylor CD, Marcus P, Wiley ECS, editors. Molecular modeling of corrosion processes. 2015.
[16] Foley RT. Role of the chloride ion in iron corrosion. Corrosion 1970;26(2):58–70.
[17] El-Naggar MM. Effects of Cl^-, NO_3^- and SO_4^{2-} anions on the anodic behavior of carbon steel in deaerated 0.50 M $NaHCO_3$ solutions. Appl Surf Sci 2006;252(18):6179–94.
[18] Ismail A, Loren NE, Abdul Latiff NF. Effect of anions in seawater to corrosion attack on passive alloys. Int J Res Eng Technol 2013;2(12):733–7.
[19] Stampella RS, Albani OA, Ruiz ER. Performance of high-alloy austenitic stainless steels in the actual and simulated bleaching media of the paper industry. Corros Sci 1993;35(1–4):289–95.
[20] Ait Addia B, Ait Addia E, Hamdani M. The effects of chloride and sulphate ions on the electrochemical behaviour of tin in aqueous solutions. Portugaliae Electrochim Acta 2018;36(1):11–22.
[21] Wang HP, Sun LF, Shi JJ, Liu CJ, Jiang MF, Zhang C. Inclusions and solidification structures of high pure ferritic stainless steels dual stabilized by niobium and titanium. Rare Met 2014;33(6):761–6.
[22] Leban MB, Tisu R. The effect of TiN inclusions and deformation induced martensite on the corrosion properties of AISI 321 stainless steel. Eng Fail Anal 2013;33:430–8.